การจำลองเชิงตัวเลขของการถ่ายเทความร้อนและการไหลด้วยการพุ่งชนของของไหลนาโนบนแหล่งกำเนิดความร้อนที่มีครีบระบายความร้อน

Numerical simulation of heat transfer and fluid flow of nanofluid jet impingement on straight fin heat sink

คมกฤษณ์ ชัยโย[1]

Khomgris Chaiyo[1]

บทคัดย่อ

งานวิจัยนี้ได้ทำการจำลองเชิงตัวเลขมาใช้เพื่อศึกษาลักษณะการถ่ายเทความร้อนและการไหลในของไหลนาโนพุ่งชนแบบราบเรียบบนแหล่งกำเนิดความร้อนที่มีครีบระบายความร้อนด้วยแบบจำลองเดี่ยว ภายใต้ขอบเขตทางความร้อนที่ครีบระบายความร้อนมีพื้นผิวร้อนแบบอุณหภูมิคงที่ ระเบียบวิธีไฟไนต์วอลุมถูกใช้เพื่อหาผลเฉลยของสมการควบคุมการถ่ายเทความร้อนและการไหลโดยใช้ของไหลนาโนอะลูมิเนียมออกไซด์ (Al_2O_3) เป็นสารทำงานที่มีความเข้มข้นโดยปริมาตรอยู่ระหว่าง 0% ถึง 4% การคำนวณได้ทำการศึกษาถึงผลกระทบของการเปลี่ยนแปลงค่าความเข้มข้นโดยปริมาตรของอนุภาคนาโนและค่าเรย์โนลด์นัมเบอร์ ผลการคำนวณที่ได้พบว่าการถ่ายเทความร้อนเพิ่มขึ้นตามค่าความเข้มข้นโดยปริมาตรของอนุภาคนาโนและค่าเรย์โนลด์นัมเบอร์ เมื่อพิจารณาจากค่านัสเซิลนัมเบอร์ ณ ตำแหน่ง Stagnation ตำแหน่งใดๆ และค่านัสเซิลนัมเบอร์เฉลี่ย นอกจากนี้ได้ทำการเปรียบเทียบชนิดของของไหลนาโนระหว่างของไหลนาโนอะลูมิเนียมออกไซด์กับของไหลนาโนไททาเนียมออกไซด์ (TiO_2) นั้นพบว่าของไหลนาโนอะลูมิเนียมออกไซด์ให้การถ่ายเทความร้อนที่ต่ำกว่าของไหลนาโนไททาเนียมออกไซด์

คำสำคัญ: การพุ่งชนระบายความร้อน, ของไหลนาโน, ครีบระบายความร้อน, อนุภาคนาโน

Abstract

The article presents a numerical investigation of heat transfer and fluid flow of the nanofluid planar jet impingement on an isothermal straight fin heat sink surface using the single-phase model. The finite volume method was used for the solution of the resulting governing equations. Al_2O_3 nanoparticles dispersed in water with the volumetric concentration of nanoparticles ranging between 0 and 4% were used as working fluid for simulating the heat transfer and fluid flow. The influences of the volumetric concentration of nanoparticles and Reynolds number were examined and discussed in detail. The results indicated that the volumetric concentration of nanoparticles and Reynolds number enhance heat transfer where considering in terms of the stagnation, the local and the average Nusselt number. Moreover, two types of nanofluid; Al_2O_3-water nanofluid and TiO_2-water nanofluid, were compared. The Al_2O_3-water nanofluid enhanced heat transfer less than the TiO_2-water nanofluid.

Keywords: Impinging jet, nanofluid, straight fin, nanoparticles

---

[1] อาจารย์ ภาควิชาวิศวกรรมเครื่องกล คณะวิศวกรรมศาสตร์ กำแพงแสน มหาวิทยาลัยเกษตรศาสตร์ วิทยาเขตกำแพงแสน นครปฐม 73140

[1] Lecturer, Department of Mechanical Engineering, Faculty of Engineering at Kamphaengsaen, Kasetsart University, Kamphaengsaen Campus, Nakhonpathom 73140

* Corresponding author: E-mail: khomgris.c@ku.th

Introduction

Impinging jets provide an effective and flexible way to transfer energy or mass in industrial applications. A directed liquid or gaseous flow released against a surface can efficiently transfer large amounts of thermal energy or mass between the surface and the fluid. Heat transfer applications include cooling of stock material during material forming processes, heat treatment (Ferrari *et al.*, 2003), cooling of electronic components, heating of optical surfaces for defogging, cooling of turbine components, and many other industrial processes (Zuckerman & Lior, 2006).

Nanofluids are a suspension of very fine solid particles or nanoparticles (length scales of 1-100 nm) which are dispersed in base fluids such as water, engine oil, and ethylene glycol (Choi & Eastman, 1995). Due to the enhancement in thermal conductivity and heat transfer provided by nanofluids compared to classical heat transfer fluids nanofluids have become drastically significant for a wide range of engineering applications which require high heat dissipation rates such as heat exchangers (Venkitaraj *et al.*, 2018) and cooling of electronic components which suffers from a high heat generation (Selvakumar & Suresh, 2012). Integrating nanofluids with an impinging jet is considered a promising technique that can overcome the challenges of heat removal (Abdelrehim *et al.*, 2019).

Several studies have investigated numerically utilizing the single-phase model under a laminar flow regime using Al_2O_3-water nanofluids. A confined impinging slot jets working with pure water or Al_2O_3-water nanofluids was numerically presented. The flow is laminar and a constant uniform temperature is applied on the target surface. The single-phase model approach was adopted in order to describe the nanofluid behavior and different particle volume concentrations. The results demonstrated that the stagnation point, the local and average Nusselt number values are increased where increasing particle concentrations and Reynolds numbers. The required pumping power ratio also are increased as growing particle concentration (Manca *et al.*, 2016).

The single- and two-phase models of Al_2O_3-water nanofluids on the hydrodynamic and heat transfer characteristics of a confined single impinging jet were studied. A laminar flow was considered with a constant heat flux on the targeted surface. The effects of Reynolds number, jet height ratio, and nanoparticle volume fraction on the local and the average Nusselt number were determined. The results demonstrated that the two-phase model exhibits higher values of local and average Nusselt number with a maximum enhancement of 150% at H/W=4 and f =4% while single phase model shows twice the pumping power obtained by the two-phase model (Abdelrehim *et al.*, 2019).

The thermal and fluid dynamic behavior of a confined two-dimensional steady laminar nanofluid jet impinging on a horizontal plate embedded with five discrete heating elements subjected to a constant surface heat flux was studied for a range of Reynolds number from 100 to 400. The results indicated that variation of inlet Reynolds number produces a significant change of the flow and heat transfer characteristics in the domain. Increasing the nanoparticle concentration from 0% to 4% exhibits discernible change in equivalent Re and Pr caused by the modification of dynamic viscosity, effective density, thermal conductivity, and specific heat of the base fluid. Substantial influence of Re is evident on Eckert number and pumping power. Eckert number is decreased whereas pumping power is increased with the growth of Re (Mookherjee *et al.*, 2020).

In order to increase the heat dissipation efficiency of electronic devices, one of the common heat dissipation methods is to use metal heat sink, such as pin-fin or plate-fin heat sink, to expand the heat exchange area and to use air duct and forced cold flow (Jeng *et al.*, 2021).

The flow and heat transfer characteristics of the liquid water-cooling performance of the micro square pin-fin heat sink were numerically studied and its geometry was optimized. The characteristics and advantages of the micro square pin-fin heat sink were compared between the square pin-fin and the column pin-fin. The results indicate that both the pin-fin porosity and located angle are important for the cooling capacity and thermal performance of the micro square pin-fin heat sink; the optimal porosity and located angle for thermal

performance are 0.75 and 30° respectively. Furthermore, the optimized micro pin-fin presents the better thermal performance than micro column pin-fin heat sink (Zhao *et al*., 2016).

A comparative experimental and numerical study were investigated on multiple-air jet impingement heat transfer characteristics in narrow channels with full-height pin fins and miniature pin fins on the target surfaces. The experiments were conducted within the Reynolds number range of 15,000-30,000. It is found that, compared to the case with flat surface, the full-height pin fins on the target surface can improve the heat transfer uniformity, and increase the overall heat transfer performance by about 32.3%, but increase the pressure loss by about 18.0%; the mini pin fins on the target surface can significantly increase the overall heat transfer performance of the jet impingement system by about 74.7%, but only slightly increase the pressure loss. Therefore, the surface with miniature pin fins can provide the most superior heat transfer performance in the jet impingement systems. Furthermore, in the numerical investigation, 3D computational fluid dynamics analysis was done to analyze the detailed flow structure and heat transfer characteristics in the jet impingement systems with different pin fin configurations (Rao, 2018).

The combination of air impingement jet arrays and arrays of target surface micro pin-fins was experimentally investigated. The effects of impingement jet Reynolds number, jet-to-target plate distance, micro pin-fin shape, and micro rectangle pin-fin height. Some interested results, when compared at a particular streamwise location, Z/D, and Re value, area-average Nusselt number ratios generally increase with height for the rectangle micro pin-fins. Besides, where Z/D = 3.0, Nusselt number ratios show heat transfer augmentations of 30 to 130 percent, which generally increase as impingement jet Reynolds number increases, but are approximately constant as streamwise row location changes (Lu *et al*., 2019)

Several studies are available on to use the air impingement jet on pin-fin heat sink, but there are a few previous investigations of using the nanofluid impingement jet. The main objective of this study is carried out to

numerically evaluate the results of heat transfer and fluid flow obtained by the single-phase model in a confined planar jet impingement using nanofluid to cool the isothermal heated surface of the straight fin heat sink. Furthermore, the influence of volumetric concentration of nanoparticles, the jet inlet Reynolds number (varied from Re=100 to 200, the flow is considered to be laminar (Manca *et al*., 2016; Mookherjee *et al*., 2020) and nanoparticle material (comparison between Al_2O_3 and TiO_2 nanoparticle types) are investigated.

Materials and methods

1. Problem description

The schematic diagram of the two-dimensional confined impinging jet system including straight fin heat sink is shown in Figure 1(a). The jet width (B) is 6 mm, the distance between the nozzle and the tip of the fins (Y) is 36 mm, and the surface length (L) is 85B mm. The specification of straight fin heat sink in this research is displayed in Figure 1(b). The following details are as the width (W) is 6.4 mm, the inter spacing (G) is 6.95 mm, the height of fins (H) is 28 mm, and the base thickness of the heat sink (t) is 4 mm. The jet impinges over the isothermal straight fin heat sink while jet inlet temperature is taken as 293 K. The isothermal straight fin heat sink has a constant temperature of 313 K. The confinement surface is adiabatic wall. The flow is considered laminar with Re vary from 100 to 200. The working fluid is Al_2O_3-water nanofluid as baseline with the volumetric concentration of nanoparticles (ø) ranged from 0 to 4%. The flow of the impinging jet is assumed to be steady, two-dimensional, laminar and incompressible. The body forces are neglected and the fluid properties are assumed to be temperature independent. Brownian motion and thermophoretic diffusions of the nanoparticles do not have any significant effect on convection heat transfer for the percentage of nanoparticle concentration considered in this study.

2. Thermophysical properties of nanofluids

The numerical simulations are performed using Al_2O_3-water and TiO_2-water nanofluids, the nanoparticle concentrations considered in the present analysis are as 0%, 1%, 2%, 3% and 4%, respectively, and not vary

spatially in each simulation. The thermophysical properties of pure water, Al_2O_3 and TiO_2 are given in Table 1. When the single-phase model is adopted in the present work as nanofluids with small nanoparticle volume concentration can be considered as Newtonian fluids for small temperature jumps (Mookherjee *et al.*, 2020). The density and the specific heat of the nanofluid are evaluated using the formula developed for conventional solid-liquid mixtures as following

$$\rho_{nf} = (1 - \phi)\rho_{bf} + \phi\rho_p \tag{1}$$

$$(\rho c_p)_{nf} = (1 - \phi)(\rho c_p)_{bf} + \phi(\rho c_p)_p \tag{2}$$

where ϕ, p_{bf}, p_b, $c_{p,bf}$ and c_p are the volumetric concentration of nanoparticles, density of the base fluid, density of the nanoparticles, specific heat of the base fluid, and the specific heat of the nanoparticles, respectively. The thermal conductivity of TiO_2-water nanofluid was found by fitting measurement data (He *et al.*, 2009).

The thermal conductivity was found by fitting measurement data by following Eqs. (3)-(4) for Al_2O_3-water and TiO_2-water nanofluids respectively (Ho *et al.*, 2010, He *et al.*, 2009

$$k_{nf} = k_{bf}(19.672\phi^2 + 2.944\phi + 1.0) \tag{3}$$

$$k_{nf} = k_{bf}(125.6\phi^2 + 4.82\phi + 1.0) \tag{4}$$

where k_{nf}, k_{bf} is the thermal conductivity of nanofluid and base fluid, respectively. The viscosity was created to fit the experimental data by following Eqs. (5)-(6) for Al_2O_3-water and TiO_2-water nanofluids respectively (Alkasmoul *et al.*, 2018)

$$\mu_{nf} = \mu_{bf} \exp(\frac{6.599\phi}{0.288 - \phi}) \tag{5}$$

$$\mu_{nf} = \mu_{bf}(25.17\phi^2 + 29.562\phi + 1.0) \tag{6}$$

where μ_{nf}, μ_{bf} is the viscosity of nanofluid and base fluid, respectively.
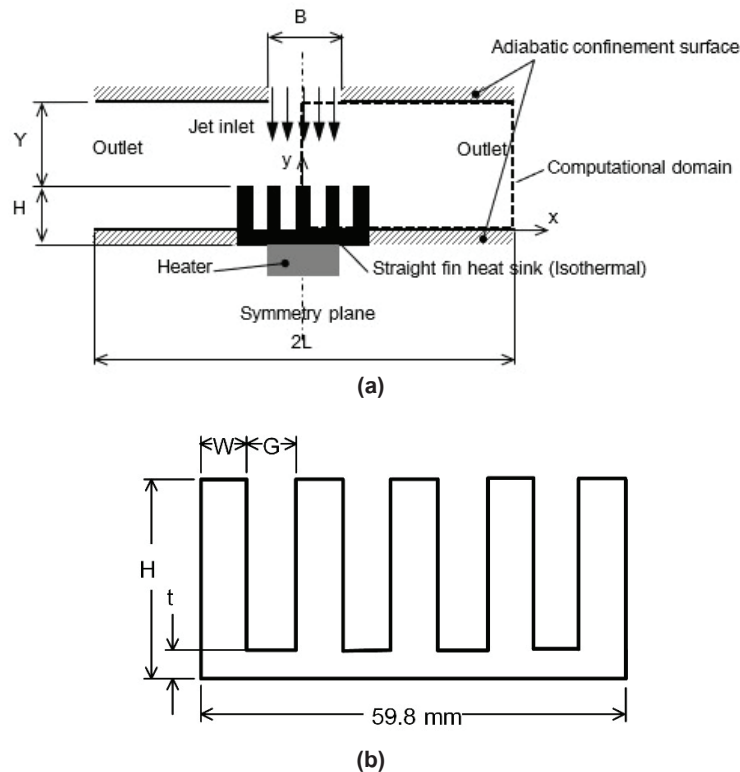

(a)

(b)

Figure 1 The confined impinging jet containing straight fin heat sink (a) two-dimensional schematic diagram (b) dimension of straight fin heat sink

Table 1 Thermophysical properties of pure water, Al_2O_3 and TiO_2 particles at T = 293 K

Material	Density ρ (kg/m³)	Heat capacity C_P (J/kg.K)	Viscosity μ (Pa.s)	Thermal conductivity λ (W/m.K)
Al_2O_3 (Oztop & Abu-Nada, 2008)	3970	765	-	40
TiO_2 (Sajadi & Kazemi, 2011)	4170	711	-	11.8
Water (Rohsenow *et al.*, 1998)	998.2	4182	993x10⁻⁶	0.597

3. Governing equations

In the present study, flows are assumed to be steady and incompressible. The governing equations include the conservation equations of mass, momentum, and energy, and can be written in the two-dimensional Cartesian coordinate system form as follows:

Continuity:

$$\frac{\partial}{\partial x_i}(\rho u_i) = 0 \tag{7}$$

Momentum:

$$\frac{\partial}{\partial x_j}(\rho u_j u_i) = -\frac{\partial p}{\partial x_i} + \frac{\partial}{\partial x_j}\left(\mu \frac{\partial u_i}{\partial x_j}\right) \tag{8}$$

Energy:

$$\frac{\partial}{\partial x_j}(\rho u_j T) = \frac{\partial}{\partial x_j}\left(\frac{\mu}{Pr}\frac{\partial T}{\partial x_j}\right) \tag{9}$$

where u_i are velocities in the streamwise and crosswise directions, T is temperature, and is pressure respectively.

4. Numerical solution procedure

The computations have been performed with the in-house developed computational code. The governing equations are solved using the finite volume method (Patankar, 1980). This scheme solves discretized versions of all equations with the non-uniform staggered grids. The principle of mass-flux continuity is improved indirectly via the solution of pressure-correction equations according to SIMPLE algorithm (Patankar, 1980). The convergence is judged by monitoring the magnitude of the absolute residual sources of mass, momentum and energy, normalized by the respective inlet fluxes. The solution is taken as having converged when all above residuals fell below 0.0001%.

The geometry of two-dimensional confined impinging jet system consists of the jet stream, straight fin heat sink, impinging and confinement surfaces as shown in Figure 1(a). Therefore, computational boundaries involved are inlet, outlet, axis of symmetry and solid walls (straight fin heat sink, impingement and confinement surfaces).

At the inlet, the jet temperature is given at 293 K. The jet stream has an almost uniform velocity profile. The Reynolds number is calculated based on jet width and mean centerline velocity as:

$$Re = \frac{\rho v_0 B}{\mu} \tag{10}$$

Next, the outlet boundary is placed at which is sufficiently far away from the main region of interest. At this boundary streamwise gradients of all variables are set to zero. Then along the axis of symmetry, the normal velocity component and the normal gradients of other variables are set to zero.

Finally, solid walls including the straight fin heat sink, the impingement and the confinement surfaces. Also, the straight fin heat sink is considered isothermal, the surface temperature of the straight fin heat sink is given at 313 K and the impingement surface and the confinement surface are adiabatic wall, respectively. The Nusselt number, is defined as:

$$Nu = \frac{-\left(\frac{\partial T}{\partial y}\right)_w B}{T_w - T_y} \tag{11}$$

Before proceeding to the discussion of the predicted results, it will be beneficial to focus first on the effect of the grid density on the solution. Figure 2 shows the computational grid 315x125 at distance x/B=67 and Y/B=3, the grid clustering is applied near the impingement surface and the straight fin surface. The grid-independency of the solutions are examined using three different grid sizes consisting of 39375 (315x125), 103750 (415x250) and 130500 (435x300) on the model Y/B=3 at Re=100 with water as working fluid. The results on the second grid 415x250 can be considered as the grid-independent results because the refinement from the grid 415x250 to grid 435x300 produces the stagnation point Nusselt number difference too small with relative error 0.59% as shown in Figure 3.
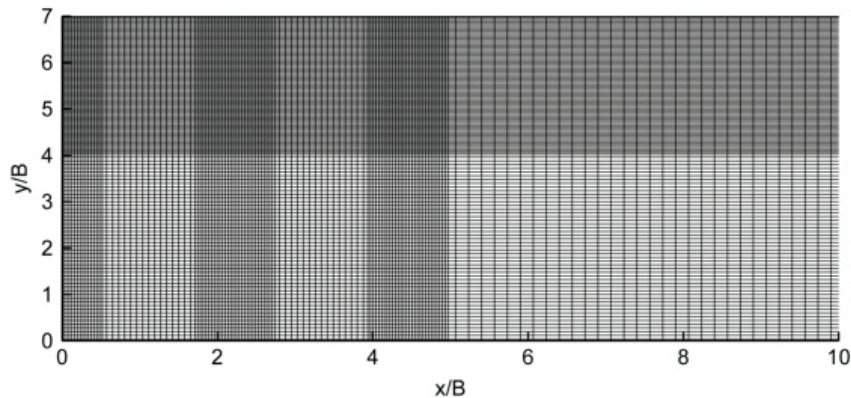
Figure 2 Sample of computational grid 315x125 (not to scale)
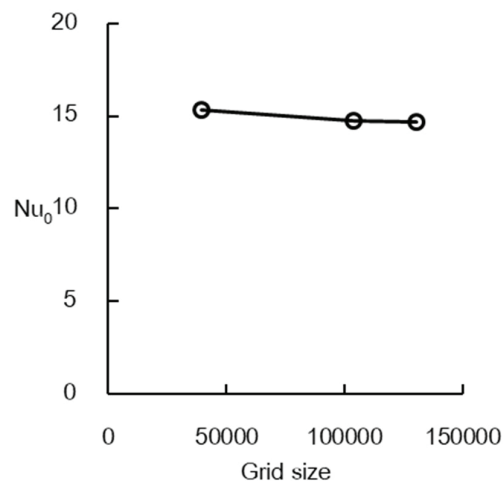
Figure 3 Grid independence test results in terms of stagnation point Nusselt number

Results and discussion

The numerical results of a two-dimensional laminar confined jet of Al_2O_3-water nanofluid impinging on the straight fin heat sink are investigated. Including the influence of volume concentration and Reynolds number are presented.

1. Numerical validation

In order to verify the developed computational code, the simulation results including the stagnation point Nusselt number and the local Nusselt number along the impingement surface in the two-dimensional confined impinging jet problem for H/B=4 were compared with the previous numerical data. The present numerical results are in good agreement with the results of Manca *et al.* (2016) and Chaiyo (2021) as shown in Table 2 and Figure 4, respectively.

Table 2 Validation of the stagnation point Nusselt number for H/B=4 and =0% in the two-dimensional confined impinging jet problem

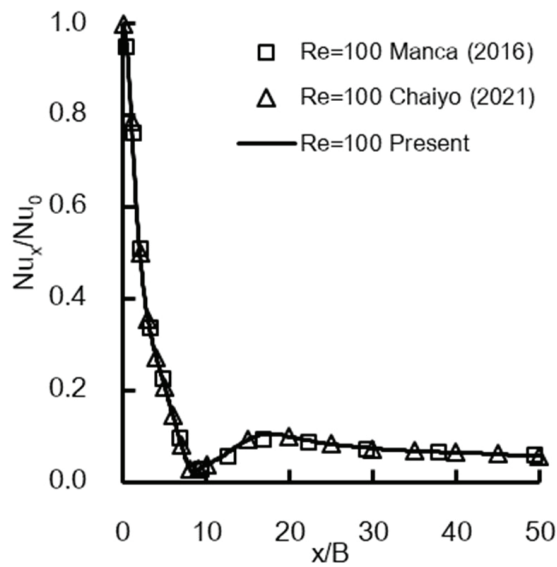| Re	$Nu_0/Pr^{1/3}$		
	Manca et al. (2016)	**Chaiyo (2021)**	**Present simulation**
100	5.66	5.67	5.67

Figure 4 Validation of local Nusselt number Nu_x profiles are scaled with the stagnation point Nusselt number Nu_0 for H/B=4 in the two-dimensional confined impinging jet problem

2. Influence of volumetric concentration

The numerical results of heat transfer and fluid flow are investigated at the different volumetric concentration of nanoparticles value as 0%, 1%, 2%, and 4% in case of Y/B=3. Figure 5 shows streamlines and isotherms in case of Y/B=3 and Re=150 at volume concentration as 0% and 4% respectively. The main jet stream impinges on the target isothermal straight fin heat sink, gets deflected, and then flows downstream in a meandering path in between the recirculation and the confinement surface toward the outlet. The developed vortices are generated by the impinging jet due to jet entrainment, confining effects, and the isothermal surface of the straight fin heat sink. The vortices are considered as main three areas as (1) the immediate vicinity of the jet and the above of the straight fin heat sink, (2) inside between straight fin heat sink-weak clockwise vortex, and (3) strong counter clockwise at downstream, respectively. Similar streamlines and isotherm trends are observed for two volumetric concentration of nanoparticles. Furthermore, the velocity vectors for Y/B=3, Re=150 and are shown in Figure 6.

Figure 7 shows the stagnation point Nusselt number (Nu_0) profiles for various volume concentrations and different Reynolds numbers. It is observed that the increased volume concentration, the Nu_0 is increased due to increasing thermal conductivity.

Figure 8 demonstrates average Nusselt number (Nu_{avg}) distribution along the periphery of the straight fin heat sink for various volume concentrations and different Reynolds numbers at Y/B=3. It is observed that the increased volumetric concentration of nanoparticles, the Nu_{avg} is increased.
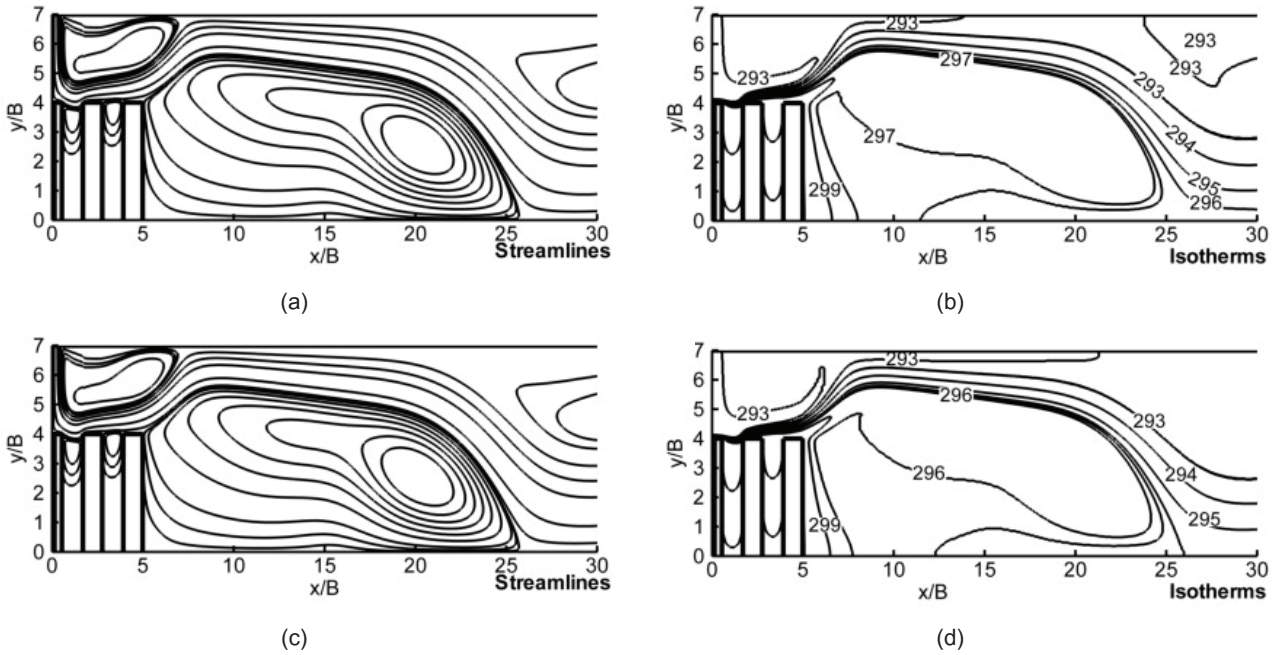
(a)

(b)

(c)

(d)

Figure 5 Streamlines and isotherms for Y/B=3 and Re=150 (a) Streamlines ∅ = 0%,
(b) Isotherms ∅ = 0%, (c) Streamlines ∅ = 4%, (d) Isotherms ∅ = 4% (not to scale)

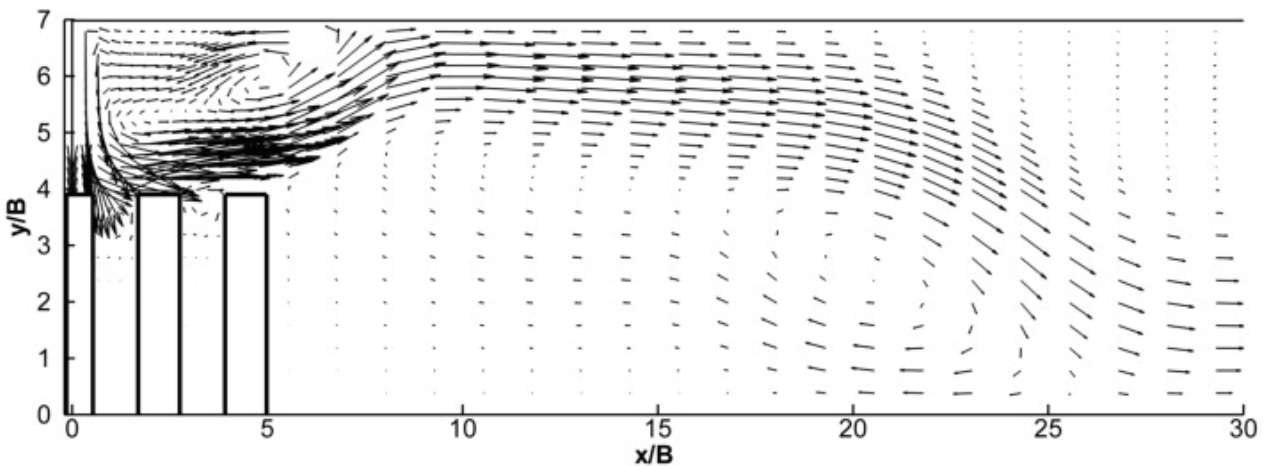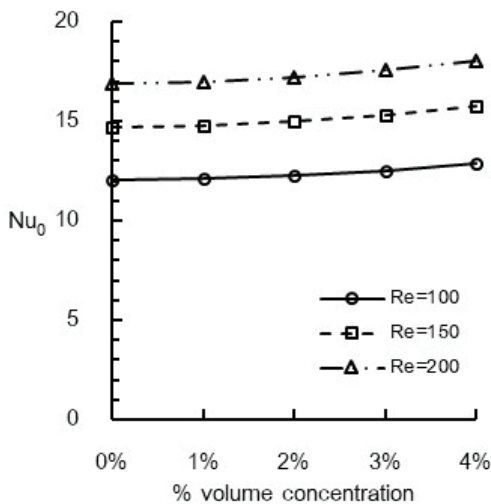**Figure 6** Velocity vectors for Y/B=3, Re=150 and ∅ = 4% (not to scale)

Figure 7 Stagnation point Nusselt number profiles for
different volume concentrations and Re numbers at Y/B=3

Additionally, Figure 9 demonstrates local Nusselt number (Nu) distribution along the periphery of the straight fin heat sink for various volume concentrations at Y/B=3 and Re=150. It is observed that increased the volumetric concentration of nanoparticles, the Nu is increased.

3. Influence of Reynolds number

Considered Reynolds number is increased from Re=100, 150, and 200 for comparison. It is found that the size of all main vortices is increased, and the secondary and the thirdly vortices are moved to downstream as shown in Figures 5(c), 10(a), and 10(c). The reattached point in the thirdly vortex is at x/B=22.5, 25.9, 28.4 for

Re=100, 150, and 200 respectively. The influence of Re onto the heat transfer can be clarified in terms of isotherms as shown in Figures 5(d), 10(b), 10(d) respectively. Additionally, the influence of Re on the heat transfer can also be seen in terms of Nu_0 and Nu_{avg} as displayed in Figures 7 and 8; these Nusselt number profiles are risen by increasing Re.
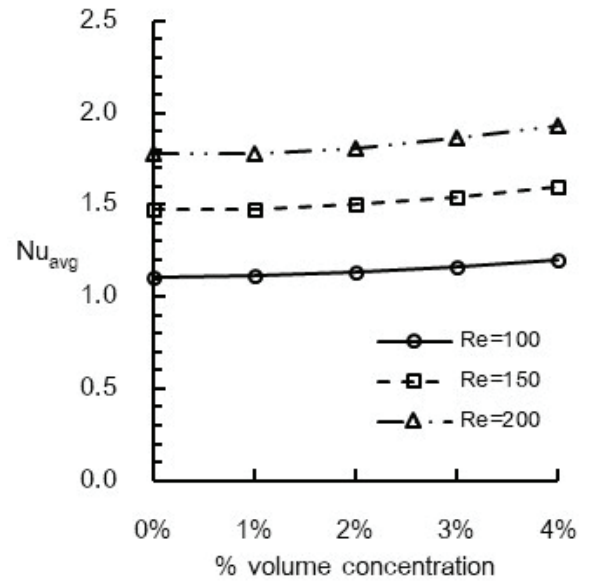
Figure 8 Average Nusselt number profiles for different volume concentrations and Re numbers at Y/B=3
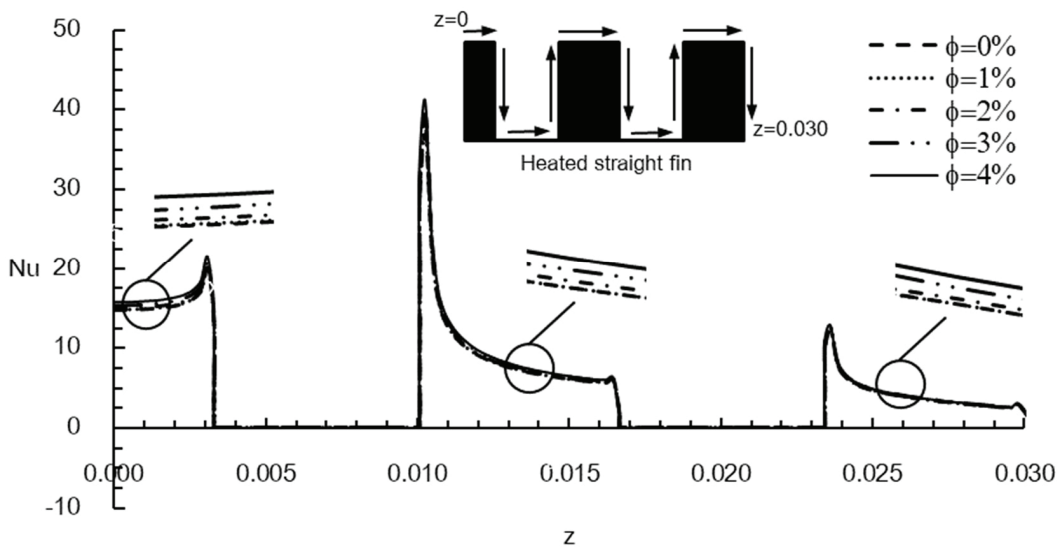
Figure 9 Local Nusselt number distribution along the periphery z of the straight fin heat sink for different volume concentrations of Al_2O_3-water nanofluid at Y/B=3 and Re=150

4. Influence of nanoparticle material

In order to compare Al_2O_3 and TiO_2 nanoparticle materials, their volumetric concentration of nanoparticles value must be same as 4%. Figure 11 shows the local Nusselt number distribution along the periphery z in each nanofluid at Y/B=3 and Re=150. It can be seen that Nu of TiO_2-water nanofluid is larger than Al_2O_3-water nanofluid and water. The difference is larger if the periphery z smaller than 0.003 m.
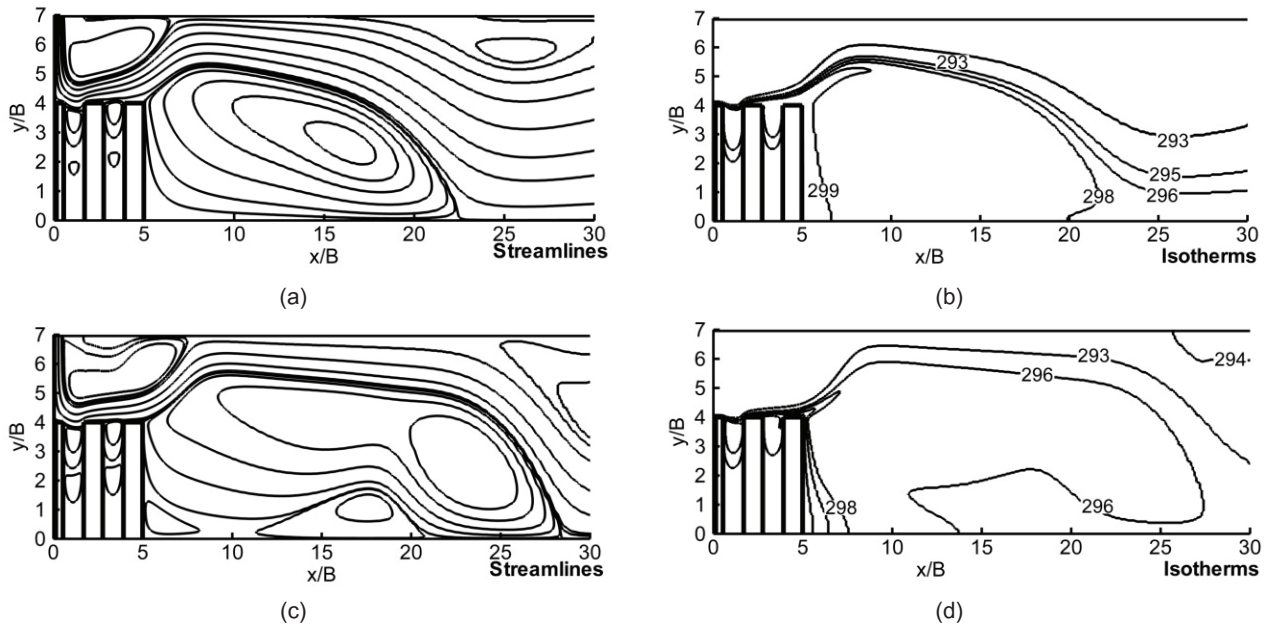
Figure 10 Streamlines and isotherms at Y/B=3, ∅ = 4%, and different Re numbers (not to scale)

(a) Streamlines at Y/B=3 Re=100, (b) Isotherms at Y/B=3 Re=100

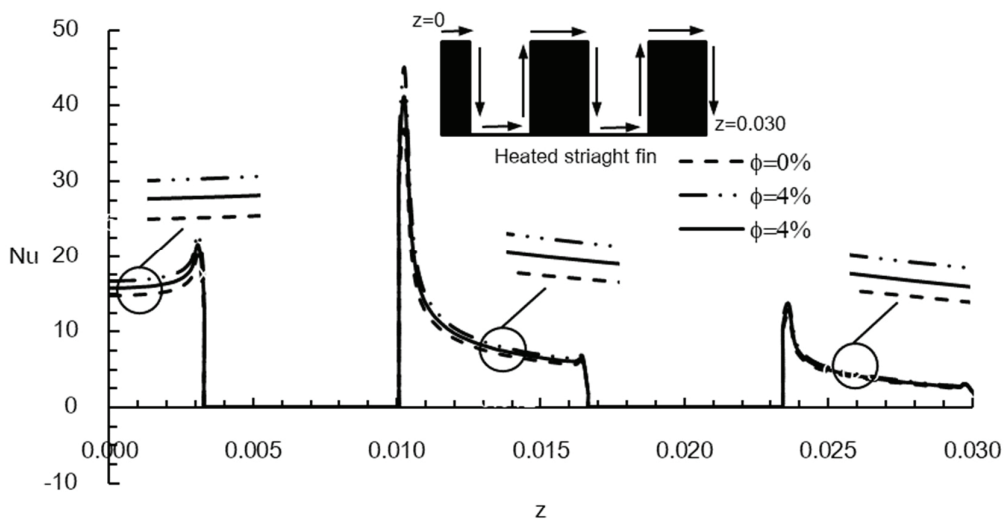(c) Streamlines at Y/B=3 Re=200, (d) Isotherms at Y/B=3 Re=200

Figure 11 Local Nusselt number distribution along the periphery z of the straight fin heat sink
for different working fluids at Y/B=3 and Re=150

Conclusion

The laminar heat transfer and fluid flow of the nanofluid jet impingement on the isothermal straight fin heat sink is numerically investigated using single-phase model. Three main objectives of this investigation are to determine the influence of volumetric concentration, Reynolds number and nanoparticle type. It is found that the volumetric concentration of Al_2O_3 nanoparticles ranging from 0 to 4% increase the heat transfer considering in terms of the stagnation, the local and the average Nusselt number. Furthermore, Reynolds number varied from 100 to 200 enhance these Nusselt numbers. The Al_2O_3 and TiO_2 nanoparticle materials are investigated, the local Nusselt number distribution along the periphery of the straight fin heat sink of TiO_2-water nanofluid is larger than Al_2O_3-water nanofluid.

Acknowledgment

References

Abdelrehim, O., Khater, A., Mohamad, A.A. & Radwan, A. (2019). Two-phase simulation of nanofluid in a confined single imping jet. *Case Studies in Thermal Engineering,14*, 100423.

Alkasmoul, F.S., Al-Asadi, M.T., Myers, T.G., Thompson, H.M. & Wilson, M.C.T. (2018). A practical evaluation of the performance of Al2O3-water, TiO_2-water and CuO-water nanofluids for convective cooling. *International Journal of Heat and Mass Transfer, 126*, 639-651.

Chaiyo, K. (2021). Numerical simulation of heat transfer and fluid flow in a confined jet impingement using water-TiO_2 nanofluid. *Journal of Science and Technology Mahasarakham University, 40*(4), 373-383.

Choi, S.U.S. & Eastman, J.A. (1995). Enhancing thermal conductivity of fluids with nanoparticles. *ASME International Mechanical Engineering Congress & Exposition, 66*, 99-105.

Ferrari, J., Lior, N. & Slycke, J. (2003). An evaluation of gas quenching of steel rings by multiple-jet impingement. *Journal of Materials Processing Technology, 136*, 190-201.

He, Y., Men, Y., Zhao, Y., Lu, H., & Ding Y. (2009). Numerical investigation into the convective heat transfer of TiO_2 nanofluids flowing through a straight tube under the laminar flow conditions. *Applied Thermal Engineering, 29*, 1965-1972.

Ho, C.J., Liu, W.K., Chang, Y.S., & Lin, C.C. (2010). Natural convection heat transfer of alumina-water nanofluid in vertical square enclosures: an experimental study. *International Journal of Thermal Sciences, 49*, 1345-1353.

Jeng, T.M., Tzeng, S.C., Tseng, C.W., & Li, Y.C. (2021). Effect of transverse synthetic jet on heat transfer characteristics of the heat sink situated in a rectangular channel with axial main flow. *Heat and Mass Transfer, 57*, 1145-1159.

Manca, O., Ricci, D., Nardini, S., Di Lorenzo & G. (2016). Thermal and fluid dynamic behaviors of confined laminar imping slot jets with nanofluids. *International Communications in Heat and Mass Transfer, 70*, 15-26.

Mookherjee, O., Pramanik, S. & Kumar Kar, U. (2020). Numerical investigation of a confined laminar jet impingement cooling of heat sources using nanofluids. *ASME Journal of Heat Transfer, 142*(8), 082301.

Lu, X., Li, W., Li, X., Ren, J. Jiang, H., & Ligrani, P. (2019). Flow and heat transfer characteristics of micro pin-fins under jet impingement arrays. *International Journal of Heat and Mass Transfer, 143*, 118416.

Oztop, H.F., & Abu-Nada, E. (2008). Numerical study of natural convection in partially heated rectangular enclosures filled with nanofluids. *International Journal of Heat and Fluid Flow, 29* 1326-1336.

Patankar, S.V. (1980). *Numerical heat transfer and fluid flow*. Hemisphere Publishing.

Rao, Y. (2018). Jet impingement heat transfer in narrow channels with different pin fin configurations on target surfaces. *ASME Journal of Heat Transfer, 140*(2), 072201.

Rohsenow, W.M., Hartnett, J.P. & Cho, Y.I. (1998). *Handbook of heat transfer* (3rd edition). McGraw-Hill.

Sajadi, A.R., & Kazemi, M.H. (2011). Investigation of turbulent convective heat transfer and pressure drop of TiO_2/water nanofluid in circular tube. *International Communications in Heat and Mass Transfer, 38*, 1474-1478.

Selvakumar, P. & Suresh, S. (2012). Convective performance of CuO/water nanofluid in an electronic heat sink. *Experimental Thermal and Fluid Science, 40*, 57-63.

Venkitaraj, K.P, Suresh, S., Alwin M., T, Bibin, B.S & Abraham, J. (2018). An experimental investigation on heat transfer enhancement in the laminar flow of water/TiO_2 nanofluid through a tube heat exchanger fitted with modified butterfly inserts. *Heat and Mass Transfer, 54*, 813-829.

Zhao, J., Huang, S., Gong, L., & Huang, Z. (2016). Numerical study and optimizing on micro square pin-fin heat sink for electronic cooling. *Applied Thermal Engineering, 93*, 1347-135.

Zuckerman, N. & Lior, N. (2006). Jet impingement heat transfer: physics, correlations, and numerical modeling. *Advances in Heat Transfer, 39*, 565-631.